Nonlinear Soft-Sensors Design for Unsteady-State VOC Afterburners

Davide Fissore
Dip. di Scienza dei Materiali ed Ingegneria Chimica, Politecnico di Torino, 10129 Torino, Italy

David Edouard
LGPC-CNRS, CPE-Lyon, 69616 Villeurbanne Cedex, France

Hassan Hammouri
LAGEP, UMR 5007, UCBL I, CPE-Lyon, 69616 Villeurbanne Cedex, France

Antonello A. Barresi
Dip. di Scienza dei Materiali ed Ingegneria Chimica, Politecnico di Torino, 10129 Torino, Italy

DOI 10.1002/aic.10602
Published online September 14, 2005 in Wiley InterScience (www.interscience.wiley.com).

An observer for a reverse-flow reactor, where the combustion of lean VOC mixtures takes place, is designed in this work and it is demonstrated to allow for a quick and reliable estimation of the inlet pollutant concentration and of the outlet reactant conversion from some temperature measurements in the reactor, even when the pollutant concentration in the feed or the pollutant itself changes and when the reaction is moving toward extinction. The results may be used for control purposes, thus avoiding expensive hardware sensors and time-consuming on-line measurements. © 2005 American Institute of Chemical Engineers *AIChE J,* 52: 282–291, 2006
Keywords: observer, reverse-flow reactor, countercurrent reactor, pseudo-homogeneous model, VOC combustion, state estimation

Introduction

Forced unsteady-state catalytic reactors were investigated in the past because it was demonstrated that temperature and composition distributions, which cannot be obtained in any steady-state regime, can be achieved by means of forced variations of some operation parameters, thus improving both conversion and selectivity in a wide range of chemical processes.[1]

A simple technical solution to achieve forced unsteady-state operation is the periodic reversal of the feed flowing direction. For an exothermic reaction, the reverse flow reactor (RFR) exhibits a heat-trap effect that can be used to achieve and maintain an enhanced reactor temperature compared to a constant-flow direction mode of operation. Under periodic flow reversal both ends of the fixed bed are used as regenerative heat exchangers. Because regenerative heat exchange is generally considered simpler and more efficient than recuperative heat exchange, the RFR has found considerable industrial application primarily for the catalytic combustion of organic pollutants in exhaust air, strongly reducing the need of auxiliary fuel to sustain the combustion, except during the start-up.[1,2]

In addition to the intrinsically dynamic behavior of the RFR, one must deal with external perturbations (in the feed concentration, composition, temperature, and flow rate), which may lead either to reactor extinction (and thus to emission of unconverted pollutants) or to catalyst overheating (and thus de-

Correspondence concerning this article should be addressed to A. Barresi at antonello.barresi@polito.it.

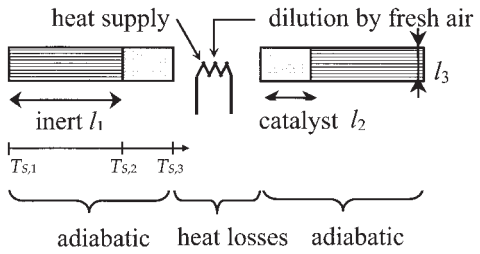

Figure 1. Main geometrical characteristics of the RFR used for the experimental validation (l_1 = 355 mm, l_2 = 75 mm, l_3 = 150 mm).

The position of the three temperature measurements used for the observer ($T_{S,1}$, $T_{S,2}$, $T_{S,3}$) is shown.

activation). To avoid these problems it is necessary to implement some closed-loop control strategy based on the measurement of the inlet concentration (and composition) and the outlet conversion. Dufour et al.[3] and Dufour and Touré,[4] for example, applied a Model Predictive Control algorithm for the control of the RFR in which the inlet pollutant concentration is known, without discussing how this value is obtained: in fact, on-line measurements may be expensive and time consuming, thus introducing a delay in the control loop.

A model-based soft-sensor (observer) can be used to estimate quickly and reliably the feed composition from some temperature measurements in the reactor: the observer combines the knowledge of the physical system (model) with experimental data (some on-line measures) to provide on-line estimates of the sought states and/or parameters. The level of detail of the model is of straightforward importance in characterizing the performance of the observer: if a detailed model taking into account finite reversal frequency and reaction kinetics is used, the resulting observer may be useless for the on-line application, being too time consuming for a computer. Edouard et al.[5] designed an observer for a medium-scale RFR, using a simplified model that is the extended version of the countercurrent reactor model of Ramdani et al.[6] The main assumption of their model is that the reaction is instantaneous and under mass-transfer control: this implies that it will be impossible to predict the extinction phenomenon; conversely, the model is independent of any chemical kinetic data. Moreover, this observer was demonstrated to give correct predictions only when the reactor is fully ignited, so that, if we want to use it for control purposes, we may control catalyst overheating, but not reactor extinction and pollutant emission. This observer was used by Edouard et al.[7] in a state-space–based control system, proving the efficiency of this approach, even if the application is limited to the case of fully ignited reactor, because of the hypothesis of the model.

The aim of the study reported in this article is thus to develop further the approach of Edouard et al.,[5] removing the assumption of instantaneous, mass-transfer–controlled reaction: the resulting observer will be able to estimate the inlet concentration and the outlet conversion also when the reactor is moving toward extinction. When the assumption of instantaneous and mass-transfer–controlled reaction is removed, the model becomes dependent on the kinetic parameters. Thus the observer can also be used to estimate the kinetic parameters of the reacting mixtures, and this can be useful when these parameters change because of catalyst deactivation or changes in the feed composition.

The same system of Edouard et al.[5] will be considered because it quite representative of small-scale industrial apparatus. The packing is made of two sets of monoliths: a long inert monolith and a short catalytic one, with Pt/Al_2O_3 as a catalyst (each channel has a diameter of 1 mm). The reactor can be considered adiabatic because of the large square cross section of the monoliths[6]; conversely, heat loss through the reactor wall takes place between the monoliths in the central chamber where the electrical heater is located and where fresh air can be injected. Figure 1 sketches the main geometrical characteristics of the RFR.

The article is structured as follows: the second section describes the simplified model that was used in the observer design; in the third section the fundamentals of the observer design are given, whereas the validation is given in the fourth section.

Modeling of the RFR

The analogy between the countercurrent reactor and the RFR was used in this work to build up a simple model. This analogy was first stated by Nieken et al.[8] and was demonstrated to occur when the switching frequency is infinite. Figure 2 shows a sketch of the countercurrent reactor under study. The basic balance equations are

$$\frac{1}{\mathrm{Pe}_{ax}}\frac{\partial^2 T_S}{\partial x^2} + \mathrm{Pe}\left(\frac{T_{G,1}+T_{G,2}}{2} - T_S\right) + \frac{a_v(-\Delta H)(H/2)}{\rho_{G,0} v_0 c_{p,G}}\frac{r_{S,1}+r_{S,2}}{2}\varphi(x) = \tau\frac{\partial T_S}{\partial t} \quad (1)$$

$$\alpha\frac{\partial T_{G,1}}{\partial x} + \mathrm{Pe}(T_{G,1} - T_S) = 0 \quad (2)$$

$$-\frac{\partial T_{G,2}}{\partial x} + \mathrm{Pe}(T_{G,2} - T_S) = 0 \quad (3)$$

$$\alpha\frac{\partial \omega_{G,1}}{\partial x} + \mathrm{Pe}(\omega_{G,1} - \omega_{S,1}) = 0 \quad (4)$$

$$-\frac{\partial \omega_{G,2}}{\partial x} + \mathrm{Pe}(\omega_{G,2} - \omega_{S,2}) = 0 \quad (5)$$

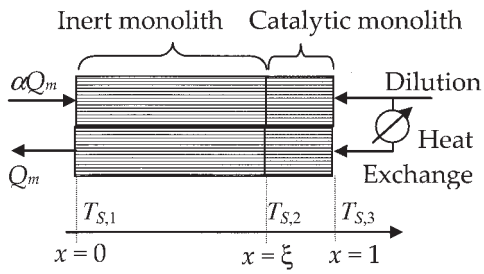

Figure 2. Countercurrent reactor model.

The position of the three temperature measurements used for the observer ($T_{S,1}$, $T_{S,2}$, $T_{S,3}$) is shown.

$$\mathrm{Pe}(\omega_{G,1} - \omega_{S,1}) = \frac{Ma_v(H/2)}{\rho_{G,0} v_0} r_{S,1} \tag{6}$$

$$\mathrm{Pe}(\omega_{G,2} - \omega_{S,2}) = \frac{Ma_v(H/2)}{\rho_{G,0} v_0} r_{S,2} \tag{7}$$

where

$$x = \frac{z}{H/2} \qquad \frac{1}{\mathrm{Pe}_{ax}} = \frac{\lambda_{ax}^S}{\rho_{G,0} v_0 c_{p,G} H/2}$$

$$\tau = \frac{(1-\varepsilon)\rho_S c_{p,S} H/2}{\rho_{G,0} v_0 c_{p,G}} \qquad \mathrm{Pe} = \frac{h a_v H/2}{\rho_{G,0} v_0 c_{p,G}} \tag{8}$$

In the model equations Nusselt and Sherwood numbers on one hand, and the Schmidt and Prandtl numbers on the other hand, have been considered to be equal, thus $h = k_D \rho_G c_{p,G}$. $\varphi(x)$ accounts for the type of monolith: $\varphi(x) = 0$ in the inert monoliths ($x < \xi$) and $\varphi(x) = 1$ in the catalytic monoliths ($x \geq \xi$). The boundary conditions for the mass balances are

$$\begin{cases} x = 0, & \omega_{G,1} = \omega_{G,0} \\ x = 1, & \alpha \omega_{G,1} = \omega_{G,2} \end{cases} \tag{9}$$

whereas the boundary conditions for the thermal balances are

$$x = 0 \qquad \begin{cases} T_{G,1} = T_{G,0} \\ \dfrac{\partial T_S}{\partial x} = 0 \end{cases}$$

$$x = 1 \qquad \begin{cases} (1+N')(T_{G,2} - T_{G,0}) = \alpha(T_{G,1} - T_{G,0}) + \dfrac{\dot{Q}_{ext}}{\rho_{G,0} v_0 c_{p,G} S} \\ \dfrac{\partial T_S}{\partial x} = 0 \end{cases} \tag{10}$$

where N' is the number of transfer units that accounts for heat loss in the central chamber.

The model given by Eqs. 1–10 is further simplified using the approach of Balakotaiah and Dommeti,[9] thus expressing the gas temperature as a function of the solid temperature: Eqs. 2 and 3 are inverted using a formal development truncated at the second-order term because the Peclet number (Pe) is much greater than unity

$$\begin{cases} T_{G,1} \cong T_S - \dfrac{\alpha}{\mathrm{Pe}} \dfrac{\partial T_S}{\partial x} + \left(\dfrac{\alpha}{\mathrm{Pe}}\right)^2 \dfrac{\partial^2 T_S}{\partial x^2} \\ T_{G,2} \cong T_S + \dfrac{1}{\mathrm{Pe}} \dfrac{\partial T_S}{\partial x} + \left(\dfrac{1}{\mathrm{Pe}}\right)^2 \dfrac{\partial^2 T_S}{\partial x^2} \end{cases} \tag{11}$$

Combining Eqs. 11 and 1 the following pseudo-homogeneous heat balance is obtained

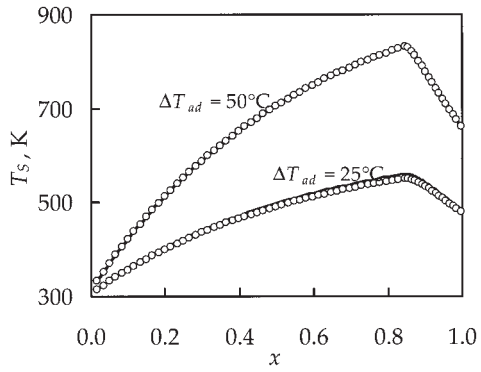

Figure 3. Comparison between the solid temperature profiles when the contribution of the downstream catalytic monolith is considered (lines) or not (symbols) for different pollutant concentration of the inlet stream.

$$\left(\frac{1}{\mathrm{Pe}_{ax}} + \frac{1+\alpha^2}{2\,\mathrm{Pe}}\right)\frac{\partial^2 T_S}{\partial x^2} + \frac{1-\alpha}{2}\frac{\partial T_S}{\partial x} + \frac{a_v(-\Delta H)H/2}{\rho_{G,0} v_0 c_{p,G}} \frac{r_{S,1} + r_{S,2}}{2} \varphi(x) = \tau \frac{\partial T_S}{\partial t} \tag{12}$$

which has to be solved with Eqs. 4–7 to obtain the temperature and concentration profiles. Further details about the model can be found in Edouard et al.[5]

The boundary conditions for the thermal balance equation are modified because now there are no longer two gas-phase first-order thermal balance equations and one solid-phase second-order thermal balance equation, but just Eq. 12. As a consequence, the boundary conditions given by Eq. 10 are expressed using Eq. 11 and truncating the developments above 1/Pe

$$\begin{cases} x = 0 & T_S - \dfrac{\alpha}{\mathrm{Pe}} \dfrac{\partial T_S}{\partial x} = T_{G,0} \\ x = 1 & (1+N')\left(T_S + \dfrac{1}{\mathrm{Pe}} \dfrac{\partial T_S}{\partial x} - T_{G,0}\right) \\ & \quad = \alpha\left(T_S - \dfrac{\alpha}{\mathrm{Pe}} \dfrac{\partial T_S}{\partial x} - T_{G,0}\right) + \dfrac{\dot{Q}_{ext}}{\rho_{G,0} v_0 c_{p,G} S} \end{cases} \tag{13}$$

It is important to highlight that the boundary conditions (Eq. 10) after the change of variables (Eq. 11) are more than those required by Eq. 12 and thus the conditions over T_S are ignored.

The contribution of the second reactor to the reaction rate, that is, $r_{S,2}$, may be neglected at least for the case of interest for the current application: in fact, if the reactor is fully ignited, the reaction may be assumed instantaneous and occurring in the upstream monolith at $x = \xi$. Even when the reactant conversion decreases and the reaction front starts moving in the upstream monolith, the contribution of the downstream monolith is generally negligible. Actually, previous studies[10] of combustion reactions in the countercurrent reactor evidenced oscillations of the reaction zone from one reactor to the other. In any event, if the reaction front reaches the downstream monolith (thus contributing to the reaction term in the mass balance) it means that the reaction is almost extinguished. Figure 3 shows a compar-

ison between the solid temperature profiles that are obtained in the reactor when the contribution of the downstream monolith is neglected or not. Equation 12, together with the mass balance Eqs. 4–7 and the boundary conditions (Eq. 13) have been solved to simulate the behavior of the countercurrent reactor for two values of the concentration of the feed. No differences are obtained in the prediction when the reactor is fully ignited, whereas there is a slight difference when the reactant conversion starts to decrease. This simplification will allow us to give to the system of equations a useful structure for the synthesis of the observer.

A first-order kinetic may be generally assumed

$$r_{S,1} = k_0 e^{-(E_a/RT_S)} c_S = k_0 e^{-(E_a/RT_S)} \frac{\omega_{S,1}\rho_G}{M} \tag{14}$$

Because of these assumptions, Eq. 12 may be rewritten as

$$\left(\frac{1}{\mathrm{Pe}_{ax}} + \frac{1+\alpha^2}{2\,\mathrm{Pe}}\right)\frac{\partial^2 T_S}{\partial x^2} + \frac{1-\alpha}{2}\frac{\partial T_S}{\partial x} + \mathrm{Pe}\,\Delta T_{ad}\frac{k_0}{k_D}\frac{\omega_{S,1}}{\omega_{G,0}}\frac{1}{2}e^{-(E_a/RT_S)} = \tau\frac{\partial T_S}{\partial t} \tag{15}$$

where

$$\Delta T_{ad} = \frac{\omega_{G,0}(-\Delta H)}{Mc_{p,G}} \tag{16}$$

The finite frequency in the RFR is responsible for a deviation with respect to the prediction based on the countercurrent model; the simple correction introduced by Edouard et al.[5] can be used to take into account the finite flow reversal frequency.

High Gain Observer

A model-based control or supervision strategy requires the knowledge of the state of the process; this may be achieved by using physical sensors. In many cases the number and type of sensors are limited because of cost consideration and physical constraints. An observer for a process described by a nonlinear dynamic system

$$\dot{x} = f(x, u) \tag{17}$$

whose observations are given by

$$y = g(x, u) \tag{18}$$

is another dynamic system,

$$\dot{\hat{x}} = f(\hat{x}, u) + \kappa[y - g(\hat{x}, u)] \tag{19}$$

having the property that the estimation error, given by

$$e = x - \hat{x} \tag{20}$$

converges to zero, independent of the state and the input. The differential equation for the error e can thus be used to study the behavior of the observer. This equation is given by

$$\dot{e} = \dot{x} - \dot{\hat{x}} = f(x, u) - f(x - e, u) - \kappa[g(x, u) - g(x - e, u)] \tag{21}$$

Suppose that by a proper choice of $\kappa(\,)$ Eq. 21 can be made asymptotically stable, that is, an equilibrium state is reached for which

$$\dot{e} = 0 \tag{22}$$

Then, in equilibrium, Eq. 21 becomes

$$0 = f(x, u) - f(x - e, u) + \kappa[g(x - e, u) - g(x, u)] \tag{23}$$

Because the righthand side of Eq. 21 becomes zero when $e = 0$, independent of x and u, $e = 0$ is an equilibrium state of Eq. 22. This implies that if $\kappa(\,)$ can be chosen to achieve asymptotic stability, the estimation error converges to zero.

The Kalman filter is often proposed in the literature for selecting the gain of an observer; the numerical difficulties involved in the design of Kalman filter–based observers can render the on-line estimation very time consuming. A different approach was used in this work, deriving the observer from the high gain techniques.[11-15] The calculation of the proposed observer gain does not require solving any differential equation and its calibration, based on a canonical form, is very simple. This section is organized as follows: first, we use the finite-difference method to approximate the reactor model by a system of ordinary differential equations; next, the resulting model is reordered to attain a particular structure that allows synthesizing the observer.

Space discretization of the system: finite-difference method

The heat balance Eq. 15 was discretized over 200 points: the same number of points was used both in the inert and in the catalytic monoliths, leading to different space discretization.[5] The discretized temperature profile is denoted by

$$X(t) = [X_1(t), X_2(t), \ldots, X_{200}(t)]^T \tag{24}$$

where

$$X_i(t) = T_S(x_i, t) \tag{25}$$

$[T_S(x_1, t), \ldots, T_S(x_{100}, t)]^T$ corresponds to the nonreactive monolith compartment and $[T_S(x_{101}, t), \ldots, T_S(x_{200}, t)]^T$ corresponds to the reactive monolith compartment. The discretization of Eq. 15, using Eqs. 4 and 6 to calculate the concentration at the solid surface, yields to the system

$$\dot{X}(t) = A[\alpha(t)]X(t) + B[\alpha(t)]U(t) \tag{26}$$

where

$$U(t) = [T_{G,0},\ Q_{ext}(t),\ \Delta T_{ad}(t)]^T$$

$$A[\alpha(t)] = \begin{pmatrix} a_4(t) & a_1(t) & 0 & \cdots & \cdots & \cdots & 0 \\ a_3(t) & a_2(t) & a_1(t) & \cdots & \cdots & \cdots & 0 \\ 0 & \ddots & \ddots & \ddots & \cdots & \cdots & 0 \\ \vdots & \ddots & a_{3c}(t) & a_{2c}(t) & a_1(t) & 0 & \vdots \\ \vdots & \ddots & 0 & \ddots & \ddots & \ddots & 0 \\ 0 & \ddots & \ddots & 0 & a_3(t) & a_2(t) & a_1(t) \\ 0 & \cdots & \cdots & \cdots & 0 & a_3(t) & a_5(t) \end{pmatrix}$$

$$B[\alpha(t)] = \begin{pmatrix} b_1(t) & 0 & 0 \\ 0 & 0 & 0 \\ \vdots & \vdots & \vdots \\ 0 & 0 & 0 \\ 0 & 0 & \dfrac{\mathrm{Pe}}{2\tau}\dfrac{k_0}{k_D}e^{-[E_a/RT_S(x_{101})]}M_c \\ \vdots & \vdots & \vdots \\ 0 & 0 & \dfrac{\mathrm{Pe}}{2\tau}\dfrac{k_0}{k_D}e^{-[E_a/RT_S(x_{199})]}M(x_{199}) \\ b_2(t) & b_3(t) & \dfrac{\mathrm{Pe}}{2\tau}\dfrac{k_0}{k_D}e^{-[E_a/RT_S(x_{200})]}M(x_{200}) \end{pmatrix}$$

The coefficients a_1, a_2, a_3, a_4, a_5, b_1, b_2, and b_3 are given in Appendix A.

The canonical structure of the system

The aim of the observer is to provide a reliable on-line estimation of the inlet pollutant concentration, that is, the ΔT_{ad}, attributed to the proportionality relationship given by Eq. 16. Following the same approach of Edouard et al.,[5] the ΔT_{ad} is considered the response of a second-order system

$$\begin{cases} \dfrac{d}{dt}\Delta T_{ad} = \zeta(t) \\ \dfrac{d}{dt}\zeta(t) = v(t) \end{cases} \tag{27}$$

where $v(t)$ is an unknown, but bounded signal.

The first goal of our observer is to estimate the inlet pollutant concentration also when the conversion is not complete; in addition, the observer should also be able to give a reliable estimation of the conversion of the pollutant in the case of kinetically controlled reaction. In this case the kinetic parameters appear explicitly in the model, but they may be unknown because of:

- change of the type of the pollutant that is fed to the reactor
- catalyst deactivation or aging
- poorly understood kinetic parameters

For these reasons, our observer should also be able to estimate the kinetic parameters of the catalytic reaction. As a consequence of the assumption of first-order kinetics, there are two kinetic parameters to be estimated, that is, the frequency factor and the activation energy. The assumption of first-order kinetics is not very restrictive, given that almost any reaction rate may be approximated by a first-order equation in a certain range of composition. For sake of simplicity we decided to keep constant the value of the activation energy and to estimate only the frequency factor; also this assumption is not limiting because for the compensation effect it is always possible to calculate a frequency factor (for a fixed value of activation energy) to obtain the value of any kinetic constant.

The formulation of this observer requires a particular structure called canonical form; the following notations are used to reorder equation system 26 into this form

$$\begin{cases} z^1(t) = [z_1^1(t),\ \ldots,\ z_{100}^1(t)]^T = [X_1(t),\ \ldots,\ X_{100}(t)]^T \\ z^2(t) = [z_1^2(t),\ z_2^2(t),\ z_3^2(t),\ z_4^2(t)]^T = \left[X_{101}(t),\ \Delta T_{ad}(t),\ \zeta(t),\ \dfrac{k_0}{k_D}\right]^T \\ z^3(t) = [z_1^3(t),\ \ldots,\ z_{99}^3(t)]^T = [X_{200}(t),\ \ldots,\ X_{102}(t)]^T \end{cases} \tag{28}$$

Because of the structure of the equations, our observer will not estimate the frequency factor k_0 but the ratio k_0/k_D. With these notations, equation system 26 can be rewritten as

$$\begin{cases} \dot{z}^1 = a_1(t)A^1z^1(t) + G^1[T_{G,0},\ \alpha(t),\ z^1(t)] \\ \dot{z}^2 = A^2z^2(t) + G^2[\alpha(t),\ z_{100}^1(t),\ z_{99}^3(t),\ z^2(t)] \\ \dot{z}^3 = A^3z^3(t) + G^3[\alpha(t),\ z^2(t),\ z^3(t),\ T_{G,0},\ Q_{ext}] \end{cases} \tag{29}$$

The matrices A and G are given in Appendix B.

The state measurements that are used to estimate the state of the system are

$$\begin{cases} y_1(t) = X_1(t) = T_S(x_1,\ t) = T_{S,1} \\ y_2(t) = X_{101}(t) = T_S(x_{101},\ t) = T_{S,2} \\ y_3(t) = X_{200}(t) = T_S(x_{200},\ t) = T_{S,3} \end{cases} \tag{30}$$

that is, the temperature at the inlet of the nonreactive monolith, the temperature at the inlet of the reactive monolith, and the temperature at the outlet of the upstream reactive monolith (in Figure 2 these three points correspond to $x = 0$, $x = \xi$, and $x = 1$).

Observer design for on-line estimation of the unknown pollutant concentration

The observer for equation system 29 takes the following form

$$\begin{cases} \dot{\hat{z}}^1(t) = a_1(t)A^1\hat{z}^1 + G^1(\hat{z}, t) - a_1(t)\Delta_{1\Omega}K^1[\hat{z}_1^1 - y_1(t)] \\ \dot{\hat{z}}^2(t) = A^2\hat{z}^2 + G^2(\hat{z}, t) - \Lambda\Delta_\theta K[\hat{z}_1^2 - y_2(t)] \\ \dot{\hat{z}}^3(t) = a_3(t)A^3\hat{z}^3 + G^3(\hat{z}, t) - a_3(t)\Delta_{3\Omega}K^3[\hat{z}_1^3 - y_3(t)] \\ y_1(t) = z_1^1(t) = T_S(x_1, t) = T_{S,1} \\ y_2(t) = z_1^2(t) = T_S(x_{101}, t) = T_{S,2} \\ y_3(t) = z_1^3(t) = T_S(x_{200}, t) = T_{S,3} \end{cases} \tag{31}$$

where the observers for the states $\hat{z}^1$ and $\hat{z}^3$ are the same as described by Edouard et al.,[5] that is

$$K^1 = \begin{pmatrix} K_1^1 \\ \vdots \\ K_{100}^1 \end{pmatrix} \quad \text{and} \quad K^3 = \begin{pmatrix} K_1^3 \\ \vdots \\ K_{99}^3 \end{pmatrix}$$

are such that the matrices

$$\bar{A}^1 = \begin{pmatrix} K_1^1 & 1 & 0 & 0 \\ \vdots & 0 & \ddots & \vdots \\ K_{99}^1 & 0 & \cdots & 1 \\ K_{100}^1 & 0 & \cdots & 0 \end{pmatrix} \quad \text{and} \quad \bar{A}^3 = \begin{pmatrix} K_1^3 & 1 & 0 & 0 \\ \vdots & 0 & \ddots & \vdots \\ K_{98}^3 & 0 & \cdots & 1 \\ K_{99}^3 & 0 & \cdots & 0 \end{pmatrix}$$

are stable, that is, the real part of their eigenvalues is negative, and $\Delta_{1\Omega}$ and $\Delta_{3\Omega}$ are, respectively, 100×100 and 99×99 matrices having the following form

$$\Delta_{1\Omega} = \begin{pmatrix} \Omega_1 & \cdots & 0 \\ \vdots & \ddots & \vdots \\ 0 & \cdots & \Omega_1 \end{pmatrix} \qquad \Delta_{3\Omega} = \begin{pmatrix} \Omega_3 & \cdots & 0 \\ \vdots & \ddots & \vdots \\ 0 & \cdots & \Omega_3 \end{pmatrix}$$

The proof of the convergence of this observer was given in Edouard et al.[5]

The observer for the state $\hat{z}^2$ was taken from Hammouri and Farza[16]; they considered a system with the following canonical structure

$$\begin{cases} \dot{r} = F(u, r) \\ y = Cr \end{cases} \tag{32}$$

where

$$F(u, r) = \begin{pmatrix} F^1(u, r) \\ \vdots \\ F^q(u, r) \end{pmatrix} \qquad r = \begin{pmatrix} r^1 \\ \vdots \\ r^q \end{pmatrix}$$

and each function $F^i(u, r)$, $i = 1, \ldots, q - 1$ satisfies the following structure

$$F^i(u, r) = F^i(u, r^1, \ldots, r^{i+1}) \tag{33}$$

Table 1. Values of the Kinetic Parameters of Some VOCs Considered in the Simulations

	Xylene	Eptane	Butylacetate
k_0, m s^{-1}	2400	50	500
E_a, J mol^{-1}	47,750	43,000	59,000

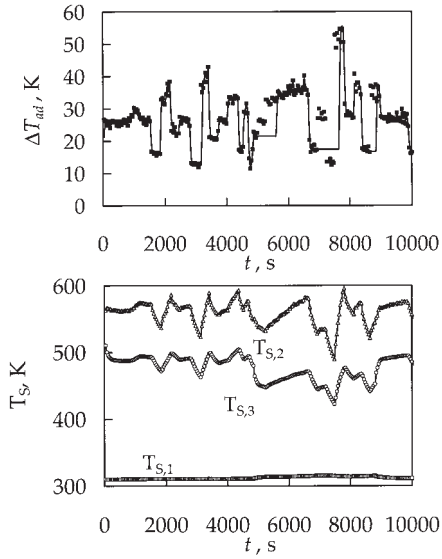

Figure 4. Comparison between the experimental measured values (symbols) and the on-line estimation (solid line) of the inlet xylene concentration, given as ΔT_{ad} (top graph) and of the solid temperatures (bottom graph) at the inlet of the nonreactive monolith (x_1), at the inlet of the reactive monolith (x_{101}) and at the outlet of the upstream reactive monolith (x_{200}) (see Figure 2).

The reactor is fully ignited.

with the following rank condition

$$\text{Rank}\left[\frac{\partial F^i(u, r)}{\partial r^{i+1}}\right] = n_{i+1} \tag{34}$$

The following functions are introduced

$$\Phi^1(u, r^1) = r^1$$

$$\Phi^k(u, r^1, \ldots, r^k) = \frac{\partial \Phi^{k-1}(u, r^1, \ldots, r^{k-1})}{\partial r^{k-1}} F^{k-1}(u, r^1, \ldots, r^k) \qquad 2 \le k \le q \tag{35}$$

The observer for equation system 32–34 takes the following form

$$\dot{\hat{r}} = F(u, \hat{r}) - \Lambda(u, \hat{r})\Delta_\theta K(C\hat{r} - y) \tag{36}$$

where F is given in Eq. 32

$$\Lambda(u, \hat{r}) = \left[\left(\frac{\partial \Phi(u, \hat{r})}{\partial r}\right)^T \frac{\partial \Phi(u, \hat{r})}{\partial r}\right]^{-1}\left[\frac{\partial \Phi(u, \hat{r})}{\partial r}\right]^T$$

with

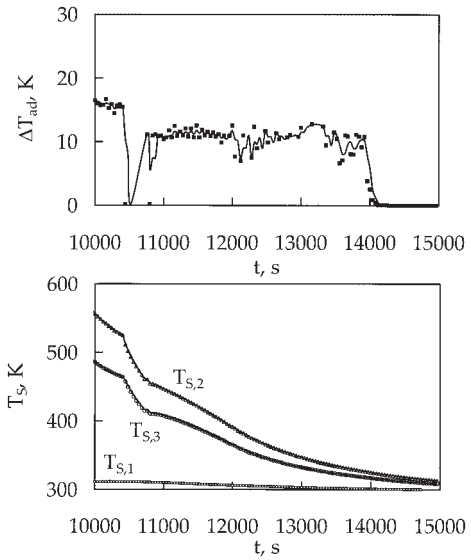

Figure 5. Comparison between the experimental measured values (symbols) and the on-line estimation (solid line) of the inlet xylene concentration (top graph) and of the solid temperatures (bottom graph) at the inlet of the nonreactive monolith (x_1), at the inlet of the reactive monolith (x_{101}) and at the outlet of the upstream reactive monolith (x_{200}).

The reactor is approaching extinction.

$$\Phi = \begin{pmatrix} \Phi^1 \\ \vdots \\ \Phi^q \end{pmatrix} \qquad \Delta_\theta = \begin{pmatrix} \theta I_{n1} & 0 & \cdots & 0 \\ 0 & \theta^2 I_{n1} & 0 & \vdots \\ \vdots & & \ddots & 0 \\ 0 & \cdots & 0 & \theta^q I_{n1} \end{pmatrix}$$

where I_{n1} is the $n_1 \times n_1$ identity matrix. K is a $qn_1 \times n_1$ constant matrix such that $(A - KC)$ is a stability matrix.

In our equation system 31

$$r^1 = z_1^2 \qquad r^2 = \begin{pmatrix} z_2^2 \\ z_3^2 \end{pmatrix} \qquad r^3 = z_4^2 \tag{37}$$

and thus $q = 3$ and $n_1 = 1$.

Validation of the Observer

Because of the low thermal capacity of the monolithic support, a low value of switching time is required to allow autothermal operation. A value of 16 s is used and is kept constant; this low value also justifies the use of the analogy with the countercurrent reactor, which is at the basis of our reactor model and thus of our observer. The pollutant is xylene; the kinetic parameters used in the model are shown in Table 1. The lid of the rig is not perfectly airtight and thus a small amount of fresh air ($\alpha = 0.95$) is aspired into the central chamber of the reactor. The sampling frequency of the thermocouples is 0.025 Hz. The following analysis was repeated also using a sampling frequency of 0.25 Hz without significant differences.

Figure 4 shows the comparison between the experimental measured values and the on-line estimation of the inlet xylene concentration and of the solid temperatures at the inlet of the nonreactive monolith, at the inlet of the reactive monolith and at the outlet of the upstream reactive monolith. The experimental values are the same as those used by Edouard et al.[5] to validate their observer. The aim of this comparison is to state, first of all, the adequacy of our observer, when the system is fully ignited. With respect to the solid temperatures, the agreement is excellent: a maximum of 1–2 K in the difference between experimental and estimated values at the boundaries between catalytic and inlet monoliths and at the inlet inert monolith and <5 K at the outlet catalytic monolith. The comparison between the estimated and the measured temperatures also demonstrates good agreement in the other point of the reactor where thermocouples were inserted. Because the solid temperatures are directly "introduced" in the observer through the measurements, the estimation is always very reliable for this state of the system, whereas for the inlet concentration—which is not measured, but only estimated—the observer exhibits its own dynamic. In any case, the inlet concentration is also properly estimated, when stiff changes take place in the steady portions with low response time.

The same comparison is repeated in Figure 5, when the reactor moves toward the extinction. It must be noted that not only the solid temperature but also the inlet concentration are properly estimated during this phase. The observer of Edouard at al.,[5] in the same conditions, gives an inlet concentration equal to zero because, being independent from any kinetic parameters, the only condition that can explain the extinction of the reactor is that the ΔT_{ad} of the feed is zero; moreover, that observer is not able to estimate the pollutant conversion. Conversely, the observer we have proposed here is able to estimate the conversion of the pollut-

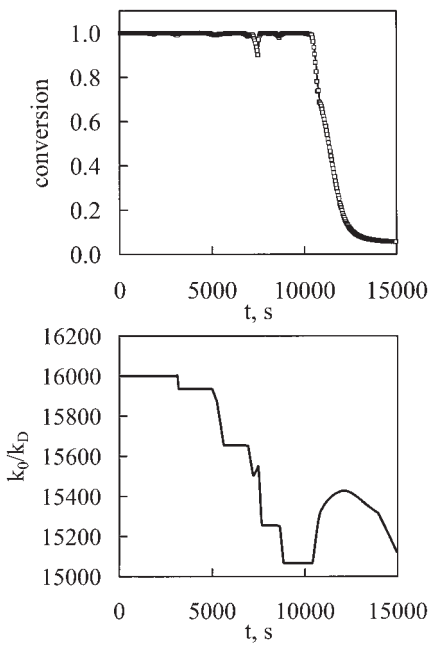

Figure 6. Comparison between the experimental measured values (symbols) and the on-line estimation (solid line) of the conversion of xylene (top graph).

Time evolution of the ratio k_0/k_D as predicted by the observer (bottom graph).

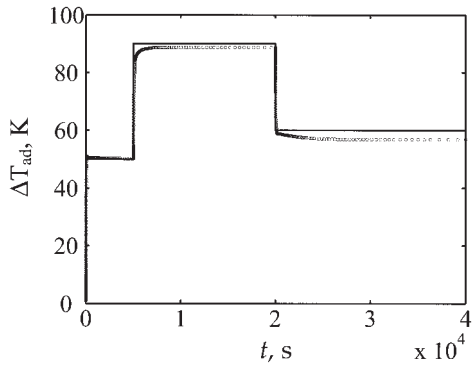

Figure 7. Comparison between the simulated values (solid line) and the observer estimation (symbols) of the inlet VOC concentration when both the VOC and its concentration change.

ant, as shown in Figure 6 (top graph). Beside the good estimation of the solid temperature profile, thus giving the value of the maximum temperature that can be used to prevent catalyst overheating, pollutant conversion is the other important parameter that must be known for control purposes. The "state" that is estimated by the observer is made up of the solid temperature, the inlet concentration, and also by the ratio k_0/k_D, given that the activation energy of the combustion reaction has been kept constant, as stated in the previous section where the observer is described. The results for the experimental run previously considered are shown in Figure 6 (bottom graph).

With respect to the maximum temperature of the solid, until the reaction remains under kinetic control, the maximum of the solid temperature is at the interface between the reactive and the inert monolith (so the value is measured). When the system approaches extinction, the maximum of the temperature continues to be located near this interface but, for control purposes, the knowledge of this value is not as important as before because the system is approaching extinction.

The proposed observer is also able to identify changes in the feed composition because both the concentration and the kinetic parameters of the pollutants are estimated. To verify this, a test has been carried out (Figure 7). In the first 6000 s xylene is fed to the reactor, and then, for 14,000 s, the feed is composed of eptane and, finally, the feed is considered to be composed of butylacetate. The prediction of the observer is obtained using the values of the solid temperatures coming from the numerical simulation of the system, instead of using the experimental values. The agreement between the "real" values and the estimation of the observer is excellent, as well as the velocity of the response of the observer.

Conclusions

The control of a reverse-flow afterburner requires the knowledge of both the solid temperature (to prevent catalyst overheating) and the pollutant conversion (to avoid pollutant emission). The proposed observer was demonstrated to give a quick and reliable estimation of the solid temperature and of the pollutant conversion, using some temperature measurements, even when we have uncertainties on the kinetic parameters.

The basis of the model used in the development of the observer is the countercurrent reactor: the analogy, as stated earlier in the text, is valid for high switching frequency even if with a simple, although empirical, correction it is possible to extend the range of switching time where the countercurrent reactor can be considered to approximate the behavior of the reverse-flow reactor. Moreover, the contribution of the second half of the reactor to the reaction has been neglected; in fact, the inclusion of this contribution poses serious problems from a theoretical perspective because it is no longer possible to attain a canonical form, but a more complex approach (Kalman filtering) should be used.

This sensor was checked in a wide range of operating conditions and was demonstrated to fulfill the requirements both when the reactor is fully ignited and when the reaction is approaching extinction and when the type of pollutant changes. This instrument can thus be used in a state-space–based control framework (such as LQR or MPC), and this will be the subject of a future work.

Notation

a_v = specific solid-gas surface area, m^{-1}
c_p = specific heat at constant pressure, J kg^{-1} K^{-1}
E_a = activation energy, J mol^{-1}
h = gas–solid heat transfer coefficient, J m^{-2} K^{-1} s^{-1}
H = length of the reactor, m
k_D = gas–solid mass transfer coefficient, m s^{-1}
k_0 = frequency factor, m s^{-1}
M = molecular weight, kg mol^{-1}
N' = number of transfer units for heat loss
Pe = Peclet number for gas–solid heat transfer
Pe_{ax} = axial Peclet number for heat conduction
$\dot{Q}_{ext}$ = external power supply, J s^{-1}
r = rate of reaction, mol m^{-2} s^{-1}
R = ideal gas constant, J K^{-1} mol^{-1}
S = total cross section of the monolith, m^2
t = time, s,
T = temperature, K
v_0 = surface gas velocity, m s^{-1}
x = nondimensional axial reactor coordinate
z = axial reactor coordinate, m

Greek letters

α = fraction of feed flow rate
ΔH = reaction enthalpy, J mol^{-1}
ΔT_{ad} = adiabatic temperature rise, K
ε = fraction of open frontal area
λ_{ax}^S = thermal conductivity of the solid, J m^{-1} K^{-1} s^{-1}
λ_{eff} = effective thermal conductivity of the solid, J m^{-1} K^{-1} s^{-1}
ξ = nondimensional position of the interface inert–catalyst
ρ = density, kg m^{-3}
τ = heat storage time constant, s
φ = parameter that accounts for the type of monolith
ω = mass fraction

Subscripts and superscripts

0 = inlet conditions
1, 2 = upstream or downstream monolith, respectively
S = solid phase or solid surface
G = gas phase

Abbreviation

RFR = reverse-flow reactor

Literature Cited

1. Matros YS, Bunimovich GA. Reverse-flow operation in catalytic reactors. *Catal Rev Sci Eng.* 1996;38:1-68.

2. Eigenberger G. Fixed bed reactors. *Ullmann's Encyclopedia of Chemical Industry*. Weinheim, Germany: VCH; 1992.
3. Dufour P, Couenne F, Touré Y. Model predictive control of a catalytic reverse flow reactor. *IEEE Trans Control Syst Technol.* 2003;11:705-714.
4. Dufour P, Touré Y. Multivariable model predictive control of a catalytic reverse flow reactor. *Comput Chem Eng.* 2004;28:2259-2270.
5. Edouard D, Schweich D, Hammouri H. Observer design for reverse flow reactor. *AIChE J.* 2004;50:2155-2166.
6. Ramdani K, Pontier R, Schweich D. Reverse flow reactor at short switching period for VOC combustion. *Chem Eng Sci.* 2001;56:1531-1539.
7. Edouard D, Dufour P, Hammouri H. Observer based multivariable control of a catalytic reverse flow reactor: Comparison between LQR and MPC approaches. *Comput Chem Eng*. 2005;29;851-865.
8. Nieken U, Kolios G, Eigenberger G. Limiting cases and approximate solutions for fixed-bed reactors with periodic flow reversal. *AIChE J*. 1995;48:1915-1925.
9. Balakotaiah V, Dommeti SMS. Effective models for packed-bed catalytic reactors. *Chem Eng Sci.* 1999;54:1621-1638.
10. Ben Tullilah M, Alajem E, Gal R, Sheintuch M. Comparison of flow-reversal and internal-recirculation reactors: Experiments, simulations, and approximations. *AIChE J.* 2003;49:1849-1858.
11. Bonard G, Hammouri H. A high gain observer for a class of uniformly observable systems. Proc of the 30th IEEE Conference on Decision and Control, Brighton, England; 1991:1494-1501.
12. Deza F, Busvelle E, Gauthier JP, High gain estimation for nonlinear systems. *Syst Control Lett*. 1992;18: 295-299.
13. Farza M, Hammouri H, Busavon K. A simple observer for a class of nonlinear systems. *Appl Math Lett.* 1998;11:27-31.
14. Gauthier JP, Hammouri H, Othman S. A simple observer for nonlinear systems. Application to bioreactors. *IEEE Trans Autom Control.* 1992; 37:875-880.
15. Gauthier JP, Kupka AK. Observability and observers for nonlinear systems. *SIAM J Control Optim.* 1994;32:975-994.
16. Hammouri H, Farza M. Nonlinear observers for local uniform observable systems. *ESAIM Control Optim Calculus Variations* 2003;9:353-362.

Appendix A

The coefficients of equation system 26 are given by

$$a_1(t) = \frac{\lambda_{eff1}}{\Delta x_k^2} \qquad a_2(t) = -2\frac{\lambda_{eff1}}{\Delta x_k^2} + \frac{D(t)}{\Delta x_k}$$

$$a_3(t) = \frac{\lambda_{eff1}}{\Delta x_k^2} - \frac{D(t)}{\Delta x_k}$$

$$a_4(t) = a_2(t) + a_3(t)\,\frac{\alpha(t)}{\mathrm{Pe}\,\Delta x_1}\,\frac{1}{1+\dfrac{\alpha(t)}{P\Delta x_1}}$$

$$a_5(t) = a_2(t) + a_1(t)\,\frac{1+N'+\alpha^2(t)}{\mathrm{Pe}\,\Delta x_2}\,\frac{1}{(1+N')\left(1+\dfrac{1}{\mathrm{Pe}\,\Delta x_2}\right)+\dfrac{\alpha^2(t)}{\mathrm{Pe}\,\Delta x_2}-\alpha(t)}$$

$$a_{2c} = (\Delta x_1 + \Delta x_2)\,\frac{\lambda_{eff1}}{\Delta x_1 \Delta x_2^2} + \frac{D(t)}{\Delta x_1}$$

$$a_{3c} = \frac{\lambda_{eff1}}{\Delta x_1 \Delta x_2} \qquad b_1(t) = a_3(t)\,\frac{1}{1+\dfrac{\alpha(t)}{\mathrm{Pe}\,\Delta x_1}}$$

$$b_2(t) = a_1(t)\,\frac{1+N'-\alpha(t)}{(1+N')\left(1+\dfrac{1}{\mathrm{Pe}\,\Delta x_2}\right)+\dfrac{\alpha^2(t)}{\mathrm{Pe}\,\Delta x_2}-\alpha(t)}$$

$$b_3(t) = a_1(t)\,\frac{1}{\rho_{G,0} v_0 c_{p,G} S}\,\frac{1}{(1+N')\left(1+\dfrac{1}{\mathrm{Pe}\,\Delta x_2}\right)+\dfrac{\alpha^2(t)}{\mathrm{Pe}\,\Delta x_2}-\alpha(t)}$$

with $\Delta x_k = x_i - x_{i-1}$.

$$D(t) = \frac{1-\alpha(t)}{2\tau} \qquad \lambda_{eff1} = \frac{1}{\tau\,\mathrm{Pe}_{ax}} + \frac{1+\alpha^2(t)}{2\,\mathrm{Pe}\,\tau}$$

and

$$M(x_i) = \prod_{k=1}^{i} \Lambda(x_k) \cdot \prod_{k=1}^{i-1} K(x_k)$$

with

$$K(x_i) = 1 + \frac{k_0}{k_D}\, e^{-[E_a/RT_S(x_i)]}$$

and

$$\Lambda(x_i) = \frac{\alpha}{\left\{1+\dfrac{k_0}{k_D}\, e^{-[E_a/RT_S(x_i)]}\right\}\{\alpha + \mathrm{Pe}\,\Delta x_2\} - \mathrm{Pe}\,\Delta x_2}$$

whereas

$$M_c = \frac{\alpha}{\left\{1+\dfrac{k_0}{k_D}\, e^{-[E_a/RT_S(x_{101})]}\right\}\{\alpha + \mathrm{Pe}\,\Delta x_1\} - \mathrm{Pe}\,\Delta x_1}$$

Appendix B

The matrices A^1 and A^3 are 100×100 and 99×99 matrices of the form

$$\begin{pmatrix} 0 & 1 & \cdots & 0 & 0 \\ 0 & 0 & \ddots & 0 & 0 \\ \vdots & \vdots & \ddots & 1 & 0 \\ \vdots & \vdots & \ddots & 0 & 1 \\ 0 & 0 & \cdots & 0 & 0 \end{pmatrix}$$

A^2 is a 4×4 matrix defined by

$$\begin{pmatrix} 0 & \dfrac{\mathrm{Pe}}{2\tau} z_4^2 (t-\Delta t) e^{-(E_a/Rz_1^2)} M_c & 0 & 0 \\ 0 & 0 & 1 & 0 \\ 0 & 0 & 0 & 0 \\ 0 & 0 & 0 & 0 \end{pmatrix}$$

where Δt is the time interval and z_1^2 can be replaced by the measured value y_2 to obtain the canonical form. The G arrays are given by

$$G^1(z,\,t)=\begin{pmatrix} G_1^1(z,\,t)\\ G_2^1(z,\,t)\\ \vdots\\ G_{100}^1(z,\,t)\end{pmatrix}=\begin{pmatrix} a_4(t)\,z_1^1+b_1T_{G,0}\\ a_3(t)\,z_1^1+a_2(t)\,z_2^1\\ \vdots\\ a_3(t)\,z_{99}^1+a_2(t)\,z_{100}^1+a_1(t)\,y_2\end{pmatrix}$$

$$G^2(z,\,t)=\begin{pmatrix} G_1^2(z,\,t)\\ G_2^2(z,\,t)\\ G_3^2(z,\,t)\\ G_4^2(z,\,t)\end{pmatrix}=\begin{pmatrix} a_{3c}(t)\,z_{100}^1+a_{2c}(t)\,z_1^2+a_1(t)\,z_{99}^3\\ 0\\ 0\\ 0\end{pmatrix}$$

$$G^3(z,\,t)=\begin{pmatrix} G_1^3(z,\,t)\\ G_2^3(z,\,t)\\ \vdots\\ G_{99}^3(z,\,t)\end{pmatrix}=\begin{pmatrix} a_5(t)+b_2(t)T_{G,0}+b_3(t)Q_{ext}\\ a_1(t)\,z_1^3+a_2(t)\,z_2^3\\ \vdots\\ a_1(t)\,z_{97}^3+a_2(t)\,z_{98}^3\\ a_1(t)\,z_{98}^3+a_2(t)\,z_{99}^3+a_3(t)\,y_2\end{pmatrix}+\begin{pmatrix} M(x_{200})\\ M(x_{199})\\ \vdots\\ M(x_{103})\\ M(x_{102})\end{pmatrix}$$

Manuscript received Mar. 11, 2005, and revision received May 23, 2005.